Numerical investigations of model support interference in a transonic wind tunnel

Sylvain Mouton

NUMERICAL INVESTIGATIONS OF MODEL SUPPORT INTERFERENCE IN A TRANSONIC WIND TUNNEL

S. Mouton[1]
ONERA, 5 boulevard Paul Painlevé, 59045 Lille Cedex, France

The aerodynamic interference effects of fin stings supporting aircraft models during wind tunnel tests have been studied by means of steady RANS simulations of the flow. The flow field and forces distortion caused by the stings were deduced by comparing simulations with and without support. Two different supports were addressed: an existing generic support and a support dedicated to the tested model and that has been designed to minimise the interference effects. Special attention was paid to the proper derivation of corrections of the incoming flow conditions in terms of Mach number and angle of attack. Comparison against experimental measurement of sting effect thanks to dummy sting tests is provided for validation purpose.

Keywords: Aerodynamic; Wind Tunnel; Sting; Support interference

Nomenclature

α	Angle of attack
CA	Axial force coefficient
CD	Drag force coefficient
CL	Lift force coefficient
CN	Normal force coefficient
Cm	Pitching moment coefficient
C_p	Pressure coefficient
FA	Axial force
FN	Normal force
M	Mach number
p	Static pressure
q	Dynamic pressure
x	Distance to MRP along model axis
$\delta\xi$	Difference of field quantity ξ due to the support $\delta\xi = \xi' - \xi$
$\Delta\xi$	Difference of integral quantity ξ due to the support $\Delta\xi = \xi' - \xi$
Subscripts	
buo	Buoyancy
nf	Near-field
ref	Flow state near model position, reference quantity
Superscripts	
'	Quantity related to 'sting on' configuration
Abbreviations	
AoA	Angle of Attack
CFD	Computational Fluid Dynamics
HTP	Horizontal Tail Plane
MRP	Model Reference Point
SCAB	Sting Calibration Body
VTP	Vertical Tail Plane
WTT	Wind Tunnel Test

[1] engineer, sylvain.mouton@onera.fr

Introduction

During wind tunnel tests the aircraft model is maintained in the test section thanks to a support system. This support is shaped to be as small and as discreet as possible, under the constraint that it should sustain forces generated over a wide range of flow conditions and enclose all cables and tubes necessary to supply energy and collect measurements from the embarked sensors. These constraints may in fact lead to supports large in size compared to the model dimensions, especially in pressurized wind tunnels where the forces on the model can reach several tons. Therefore, it is generally recognized that aerodynamic interference caused by the model support may have a significant effect on the measured data [11][12][13] and several studies were undertaken as early as in the 50s (and probably before) [9][16][17] and more recently [5][9][10][15] to determine this effect for numerous configurations and flow velocities.

In most wind tunnel procedures, the support effect is now accounted for thanks to various correction methods [7][8][14]. Unfortunately, the presently existing methods exhibit several drawbacks:

- they differ from one wind tunnel to another, making it difficult to compare results;
- they rely on simplifying hypotheses and/or empirical assumptions, which validity is doubtful for example at high Mach numbers or for unconventional models;
- they call upon dedicated experiments which are touchy, expensive and requires the introduction of another support, i.e. additional distortions of the flow.

In an attempt to alleviate these drawbacks, several recent [3][4][5] or older [9] initiatives aimed at determining whether advanced numerical simulations could help in understanding and predicting the support interference effect.

This paper summarises such an attempt carried out at ONERA within the FLIRET (FLIght REynolds number Testing) European project. It addresses the case of a transonic transport aircraft mounted on two different fin stings in ETW (European Transonic Wind tunnel) cryogenic wind tunnel as depicted in Figure 1. The first sting called *Existing Fin Sting* (EFS) is made of an already available generic sting and blade. The second sting, called *Optimised Fin Sting* (OFS) was designed for this model with the objective to minimise flow distortion on the model.

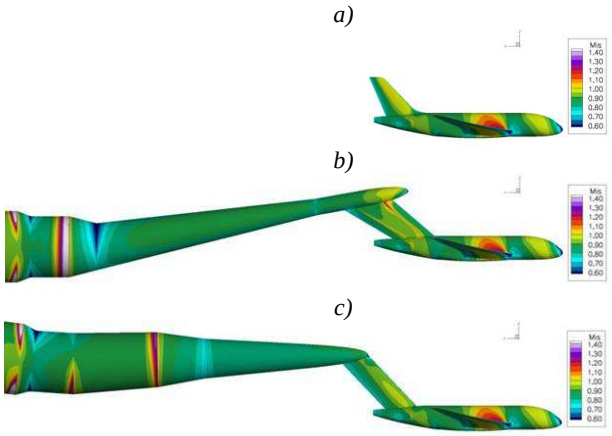

Figure 1: View of model and supports coloured by isentropic Mach number at M_{ref}=0.85, α_{ref}=1.54°
a) Remfi model
b) with existing fin sting (EFS)
c) with optimised fin sting (OFS)

1. Numerical simulations

a. *Aircraft model and meshes*

The model used for this study is a wing-body configuration with a vertical tail plane (VTP). It includes the REMFI fuselage and the wing of the HiReTT model [6]. It is representative of a large modern transport aircraft.

The simulated shape of the model closely represents the deformed wing shape under loads corresponding to cruise conditions. The geometry of the fin-sting supports includes the complete sting line down to the sector interface. The sector itself is considered to be part of the empty wind tunnel and is not included in the simulation. Besides, it was shown that a large part of its effect is in fact compensated by proper divergence of the wind tunnel walls [4]. The supports are terminated downstream by a slant fairing to avoid flow separation that would hinder convergence of the computations. The wind tunnel walls are not modelled considering the difficulty to properly simulate the flow in the floor and ceiling slots.

This work made use of the Chimera method that enables to deal with overset grids. A 8-million cell mesh of the isolated aircraft including the VTP was first generated and is shown in Figure 2. This mesh is used to compute the flow field without any support. For each sting under study, a mesh of the support was then generated and overset with the original aircraft mesh using Chimera method. The Chimera method makes the remeshing process much easier when a support is added or modified, and permits to keep the spurious mesh effects as low as possible. However, dedicated post-processing methods are required to properly integrate surface forces in area where the model skin is defined several times, by different overset meshes.

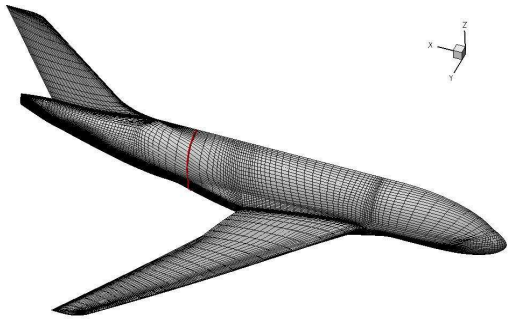

Figure 2: Surface mesh of Remfi model
1 point out of 2 is displayed for clarity. Red line indicate separation between front body and rear body

b. *Flow modelling and numerical details*

Steady RANS equations are used to model the fully turbulent flow-field around the aircraft model and support. The Mach number and AoA were in the range 0.80 to 0.87 and 0° to 3° respectively. For all computations, the Reynolds number based on mean aerodynamic chord (MAC) was $32.5\ 10^6$. The one-equation Spalart-Allmaras turbulence model was selected for all computations due to consolidated experience with this model on this kind of configuration. The boundary layer was modelled on the aircraft and on the blade surface thanks to proper boundary conditions and mesh refinement. On the contrary, no viscous effect is modelled on the sting, apart from the blade. No reflection boundary condition was used on the far-field surfaces. Flow equations were solved using *elsA* software [1]. Mean flow equations were solved thanks to a Jameson second order spatial scheme, using coefficients of artificial dissipation of 0.25 for second order and 0.008 for fourth order, and Martinelli correction with an exponent of 0.3. Iterative method for time marching was a first order backward Euler scheme, associated with implicit scalar LU-SSOR solving with 4 relaxation cycles. To improve convergence, local timestep and a 3-level multigrid cycle were used, except when using Chimera method that obliges to restrain the multigrid method to one level of coarse grid.

2. Wind tunnel tests

a. *Facility*

The European Transonic Wind tunnel (ETW) located in Cologne, Germany, is a modern cryogenic

test facility covering subsonic, trans- and supersonic regimes (Mach 0.15 to 1.35). By testing model in a very cold pressurized nitrogen flow (temperature down to 110 K and pressure up to 4.5 bars), this facility is able to simulate Reynolds numbers close to actual flight conditions. A further advantage of the pressure and temperature control is that Reynolds and deformation effects can be studied independently.

The test section is 2.4 m wide, 2.0 m high and 9.0 m long. The top and bottom walls include six slots each to minimize wall interference and blockage at transonic speeds. During the tests of full span models, the model is hold in position by a sting attached to the sector enabling AoA variations. The high attainable pressure level in this tunnel imposes the choice of support larger than usual to sustain forces on the model in the full range of working conditions. Therefore, support interference is expected to be large, which make this case ideal for CFD validation.

b. Twin-sting tests

In order to assess the effect of model supports on the aerodynamic force coefficients and flow-field, a dedicated experiment with a dummy sting was realised in ETW. During this test, the model is hold in the tunnel thanks to a so-called twin sting rig, which consists in two straight booms, holding the model by the wing lower side (see Figure 3). In reference configuration, the VTP is installed and data are acquired for different flow conditions. Then the VTP is removed and the dummy sting is installed. This dummy sting has the same shape and position as the real sting which effect is investigated. Performing tests for the same flow conditions permits to deduce the dummy sting effect by subtraction.

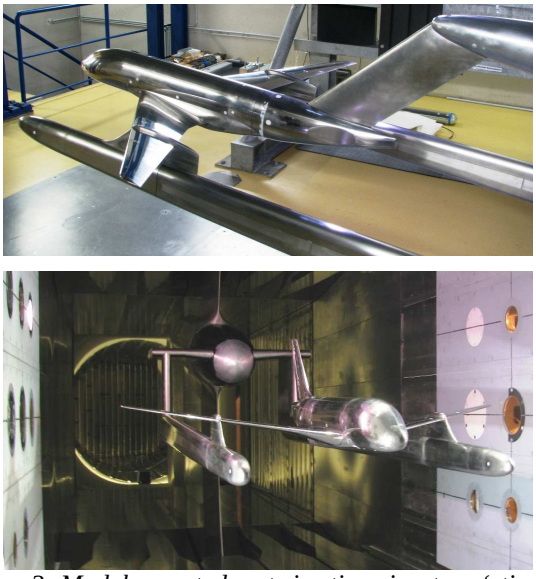

Figure 3: Model mounted on twin sting rig ; top: 'sting on' configuration in preparation room; bottom: sting off' configuration in ETW test section

For this test, the fuselage was split between front body and rear body as shown in Figure 2. Forces on the rear body were measured thanks to a six-component balance installed in the fuselage, while forces on the complete model (plus the front end of the twin-sting booms) were measured thanks to two six-component balances installed in the twin-sting booms. The model was also equipped with static pressure taps placed mostly on the fuselage. In order to perform cavity and split plane corrections, the pressure inside the model was also measured.

Due to budget constraints, only the dummy OFS was manufactured and tested and therefore data for OFS effect only are available. Also for budget and mechanical constraints, the tests were carried out at ambient temperature and pressure, yielding a Reynolds number of $4\,10^6$ based on MAC. Consequently, transition was imposed on the wing, fuselage and VTP. The Mach number was in the range 0.83 to 0.87.

3. Principles of sting support corrections

a. Definition of upstream flow corrections

The first main difficulty arising when considering an aircraft model surrounded by disturbing hardware (such as a support, wind tunnel walls or probe) is to identify a set of equivalent freestream conditions to which one can attribute the measured forces and subsequently make them non dimensional. In the present case the volume of the downstream support slows the flow down and generates downwash near the model, compared to incoming flow. Therefore, in order to blow the model at a given Mach number M_{ref} and a given AoA α_{ref}, it is necessary to correct upstream flow conditions by an amount ΔM and $\Delta\alpha$ to retrieve near the model $M_{ref} = M' + \Delta M$ and $\alpha_{ref} = \alpha' + \Delta\alpha$ as sketched in Figure 4.

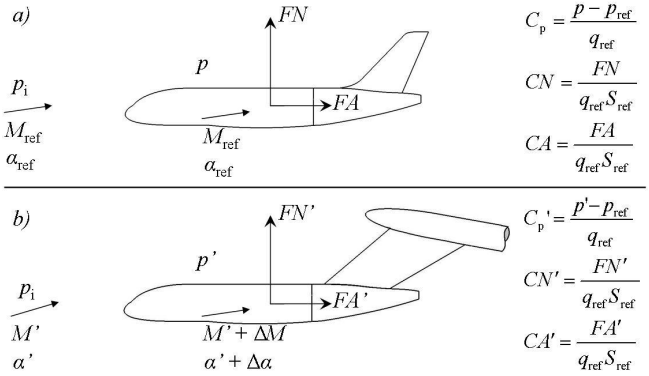

Figure 4: Definition of configurations and force nomenclature
a) model without sting (free flight)
b) model with sting

Since the distortion field generated by the support is highly inhomogeneous, an unquestionable definition of the set of corrections ΔM and $\Delta\alpha$ is highly difficult to pose. Guidelines for this definition rely on the small disturbance assumption, which is

reasonable as long as the support is moderately intrusive with respect to the model. Under this hypothesis the flow field around the support can be described by the linearised potential equation, and linearly added to the flow field generated by the model itself. The searched corrections may then be extracted from this three-dimensional distortion field thanks to some averaging process.

b. Determination of upstream flow corrections

Methods relying on solutions of the linearised potential equation are still widely used at present time in numerous wind tunnels. The potential flow field around the support is numerically solved, and the searched corrections are probed at some point of the model (such as ¼ of MAC), or are chord-weighted averaged along the wing span. This method is inexpensive and flexible. However, it suffers from the hypotheses of the linearised potential equation and may become inappropriate in cases when this equation can hardly be applied, i.e. at high Mach numbers and close to the support stagnation areas.

On experimental side, it is also possible to directly measure a subset of the support distortion field in the wind tunnel thanks to careful calibration tests, during which the support is installed in the tunnel, and then removed. To some extent, dummy sting tests may serve this purpose. Although this method less suffers from theoretical limitations, measurements are often limited to the tunnel centreline and to the Mach number. It is indeed difficult in practice to measure with sufficient accuracy the flow angle generated by the support.

Since no universal method or definition for the derivation of the Mach number and AoA corrections could be found, it was attempted during this research work to test a variety of possible values, and to identify the best solution thanks to a quality criterion. The results of this investigation will be presented in section 4.

c. Sting effect on forces

In computations as in experiments, the reference configuration, i.e. the 'sting off' configuration, includes the VTP. In 'sting on' configuration, the sting replaces it, with the hope that the blade interference effect onto the fuselage is close to the original VTP effect, hence reducing flow distortion on the rear fuselage. The sting interference effect is here defined as the difference in wing and fuselage forces between 'sting off' and 'sting on' configuration.

Once a definition for the Mach number and AoA correction is established following the arguments of previous subsection, the reference static and dynamic pressures p_{ref} and q_{ref} can be computed from the tunnel total pressure p_{i}:

$$p_{\text{ref}} = p_{\text{i}}\left(1+\frac{\gamma-1}{2}M_{\text{ref}}^2\right)^{\frac{\gamma}{1-\gamma}}$$

$$\text{and } q_{\text{ref}} = \frac{\gamma}{2}p_{\text{ref}}M_{\text{ref}}^2 .$$

The normal and axial forces *FN* and *FA* on the model skin can then be made non-dimensional to derive coefficients *CN* and *CA*. Then, force coefficients are projected onto the wind axes to derive drag coefficient *CD* and lift coefficient *CL* using the corrected AoA α_{ref}. Force coefficients can therefore be written in 'sting off' configuration as:

$$CD = \frac{FA}{q_{\text{ref}}S_{\text{ref}}}\cos\alpha_{\text{ref}} + \frac{FN}{q_{\text{ref}}S_{\text{ref}}}\sin\alpha_{\text{ref}}$$

$$CL = \frac{FN}{q_{\text{ref}}S_{\text{ref}}}\cos\alpha_{\text{ref}} - \frac{FA}{q_{\text{ref}}S_{\text{ref}}}\sin\alpha_{\text{ref}}$$

and in 'sting on' configuration:

$$CD' = \frac{FA'}{q_{\text{ref}}S_{\text{ref}}}\cos\alpha_{\text{ref}} + \frac{FN'}{q_{\text{ref}}S_{\text{ref}}}\sin\alpha_{\text{ref}}$$

$$CL' = \frac{FN'}{q_{\text{ref}}S_{\text{ref}}}\cos\alpha_{\text{ref}} - \frac{FA'}{q_{\text{ref}}S_{\text{ref}}}\sin\alpha_{\text{ref}} .$$

The sting effect on model forces are then:

$$\Delta CD = CD' - CD$$

$$\Delta CL = CL' - CL$$

Same definition stands for pitching moment effect ΔCm.

With this definition, if the distortion field generated by the support was sufficiently homogeneous all over the model, the simple fact of taking into account the proper deviations ΔM and $\Delta\alpha$ with respect to free-stream conditions would be enough to exactly retrieve the free-flight forces and one would have $\Delta CD = \Delta CL = \Delta Cm = 0$.

4. Derivation of Mach number and AoA corrections

a. Corrections minimizing wing pressure distortion

In order to investigate the effect of Mach number and AoA corrections, a quality criterion was chosen to quantify the difference in wing flow-fields between the free-flight configuration and the configuration with support. This criterion *J* is the RMS of pressure deviations of the wing, i.e. the L_2-norm of wing field $\delta C_{\text{p}} = C_{\text{p}}' - C_{\text{p}}$:

$$J(\Delta M, \Delta\alpha) = \sqrt{\int_{\text{wing}} \left(\delta C_{\text{p}}\right)^2 \frac{dS}{S_{\text{wing}}}} .$$

A full exploration of the $(\Delta M, \Delta\alpha)$ space in the range $[-0.010\ ,\ 0]\times[-0.1^{\text{o}}\ ,\ 0^{\text{o}}]$ was then realised, both for EFS and OFS. Free-flight flow condition for this test case were $M_{\text{ref}} = 0.85$ and $\alpha_{\text{ref}} = 1.54°$, corresponding to $CL = 0.50$. Results were interpolated between samples thanks to a Kriging method and are displayed in Figure 5.

Results clearly show there exists an optimal set of corrections (ΔM, $\Delta\alpha$) for representative wing flow. Looking at pressure distribution on the wing reveals that J is primarily sensitive to the shock wave position, which is mainly driven by the Mach number in the flow condition under study and for this wing design. It explains why the J-criterion is much more sensitive to this variable. J-optimal corrections are summarised in the table 1.

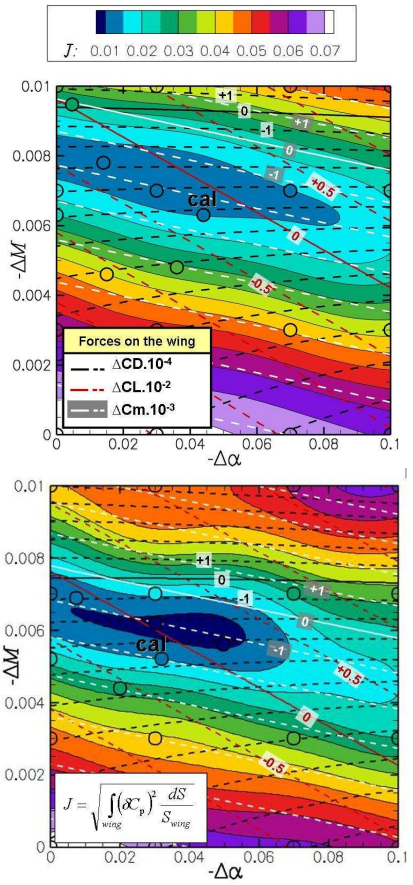

a) EFS

b) OFS

Figure 5: RMS of wing pressure distortion and wing force increments generated by EFS (a) and OFS (b) for various ΔM and Δα. Circles indicate sampled points, 'cal.' indicates SCAB calibration method (see section 4b), model forces are projected using α_{ref} whatever the AoA correction, Kriging interpolation between samples.

	EFS			OFS		
	ΔM 10^3	$\Delta\alpha$ 10^2 °	J 10^2	ΔM 10^3	$\Delta\alpha$ 10^2 °	J 10^2
J-Optimum	-7.3	-3.3	1.16	-6.0	-4.3	0.83
Calibration	-6.3	-4.4	1.48	-5.2	-3.2	1.48

Table 1: Corrections to upstream flow conditions according to different methods

	EFS			OFS		
	ΔCD 10^4	ΔCL 10^2	ΔCm 10^3	ΔCD 10^4	ΔCL 10^2	ΔCm 10^2
J-Optimum	-3.5	-0.1	-1.8	-2.1	0.0	-1.0
Calibration	-5.0	-0.2	-2.3	-3.7	-0.2	-2.0

Table 2: Sting effect on forces according to different methods

It can be seen that the OFS design can achieve a weak improvement (−28%) of the RMS-averaged level of distortion, provided the Mach number correction is carefully adapted to the support used, with accuracy of the order of 10^{-3}. Even in this case, a residual discrepancy of around 0.01 in pressure coefficient remains, most of which originates from the shock wave area, since the shock position and intensity cannot be exactly reproduced on the whole span when sting is installed, as depicted in Figure 6.

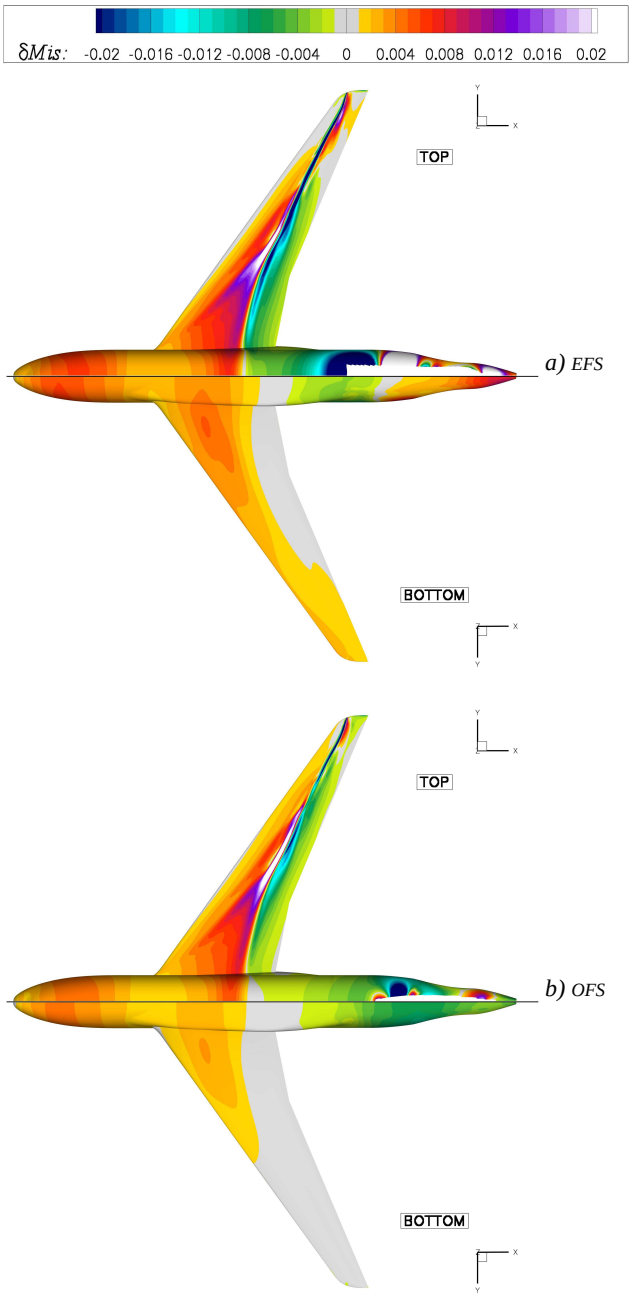

a) EFS

b) OFS

Figure 6: Distortion of isentropic Mach number on model skin due to EFS (a) and OFS (b) at M_{ref} = 0.85 and α_{ref} = 1.54° with J-optimum corrections on Mach and AoA

Concerning sting effect on forces, at optimal Mach number and AoA correction, the support effect on lift vanishes (ΔCL less than 0.001) but there is still a residual difference in the drag and in the pitching moment of the wing as summarized in table 2. Here

again, this residual level of distortion is slightly reduced when using the OFS instead of the EFS. One should note that drag deviation in the Figure 5 is weakly dependent on $\Delta\alpha$ because flow angle correction is not used in the projection of forces, since the correct AoA α_{ref} is already known. This is not the case during wind tunnel tests and $\Delta\alpha$ has to be carefully determined, since as a rule of thumb an error of 0.01° implies a drag deviation of 10^{-4} at a 0.5 lift coefficient.

b. Calibration method

Although it permits to identify optimal Mach number and AoA corrections, the systematic exploration of numerous possible corrections requires performing one CFD computation per sample, i.e. about 20 computations per polar point. Therefore, alternatives methods were explored to find a less expensive way. The only method presented in this paper mimics the calibration test of the tunnel section. It is indicated in previous figures and table under the name 'calibration'. This method was selected to derive the results presented in the rest of this paper, and it is presented hereafter.

The calibration method consists in performing simulations on the calibration body of the wind tunnel, called the SCAB. This body is a cylinder with blunt nose of diameter 160 mm, equipped with four rows of pressure taps on top, bottom and on each side. It can be mounted on different supports and is used to calibrate the tunnel, i.e. to measure the pressure (and hence velocity) distribution on the tunnel centerline for different configurations and flow conditions.

On simulation side, a Euler computation of the isolated calibration body is first performed. Then, the body is simulated mounted of the support under study (Figure 7). Both computations are carried out in free-flow, i.e. without simulation of slotted wind tunnel walls. By subtraction, one can deduce a perturbation field that can be attributed to the support (Figure 8). From this perturbation field, the Mach number and AoA correction are extrapolated at the model reference point (MRP), i.e at the ¼ MAC abscissa on the model centerline.

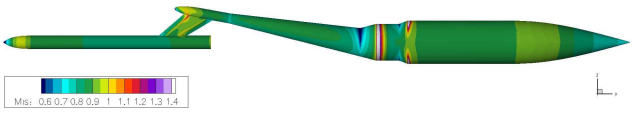

Figure 7: SCAB calibration body mounted on EFS

It may be noted that similar computations of sting distortion field served as a basis to design the OFS. The result of this design work is visible in Figure 8 under the form of a reduction of flow inhomogeneity at the wing location, compared to EFS.

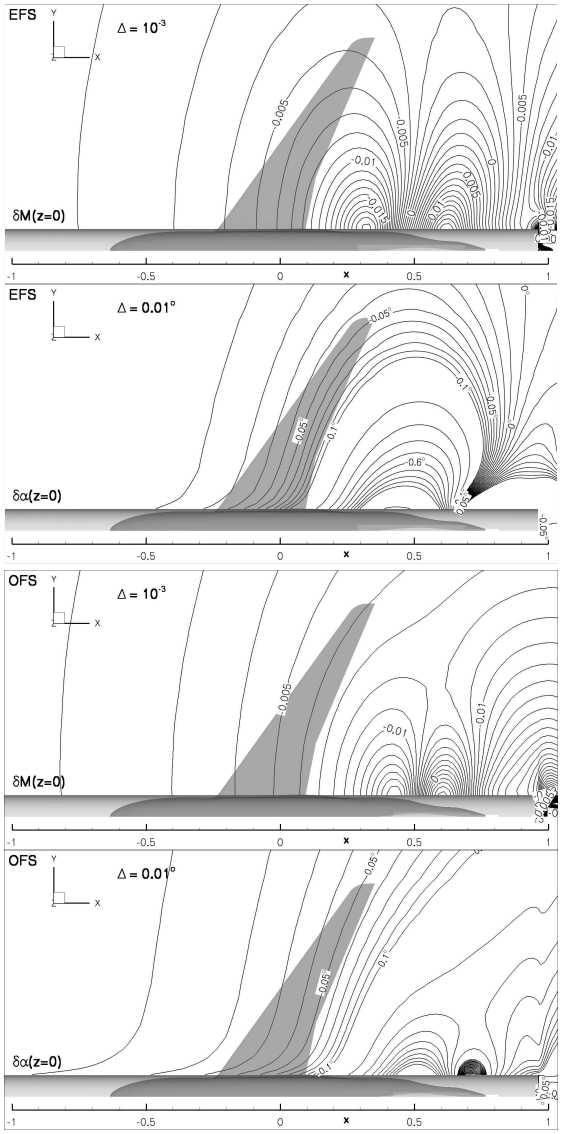

a) EFS

b) OFS

Figure 8: Distortion field generated by EFS (a) and OFS (b) at M' = 0.85 and α' = 0°; top: Mach number distortion; bottom: flow angle distortion

A comparison of these computations with experimental data is available from a previous study for which measurements were available on a straight sting and a blade-sting support (called Z-sting) similar to the ones of this paper. Figure 9 shows that the pressure distribution caused by the straight and Z-sting supports are very well predicted (within 10^{-3} Mach). These results demonstrate that the divergence of the wind tunnel walls is properly set, creating no velocity gradient on the centreline. For this low-blockage (0.42%) non-lifting case, the wall effect is also negligible.

As can be seen from Figure 5, this method yields results close to the optimum corrections. Considering the agreement between experiments and CFD this indicates that the experimental calibration procedure is also close to the optimum correction in terms of Mach number. Unfortunately, no data on flow angle correction can be experimentally measured or inferred, which is considered a large drawback of this calibration method. Furthermore,

although probing flow distortion on the tunnel centerline and taking the value at ¼ MAC was satisfactory for this model configuration, it may not be the case for unconventional configurations. Indeed, the classical 30° swept wing is found to follow iso-lines of flow distortion as shown in Figure 8, in such a way that probing data on the centerline or averaging all along the wing span yields about the same result. This would not be the case for example on a swept back wing configuration.

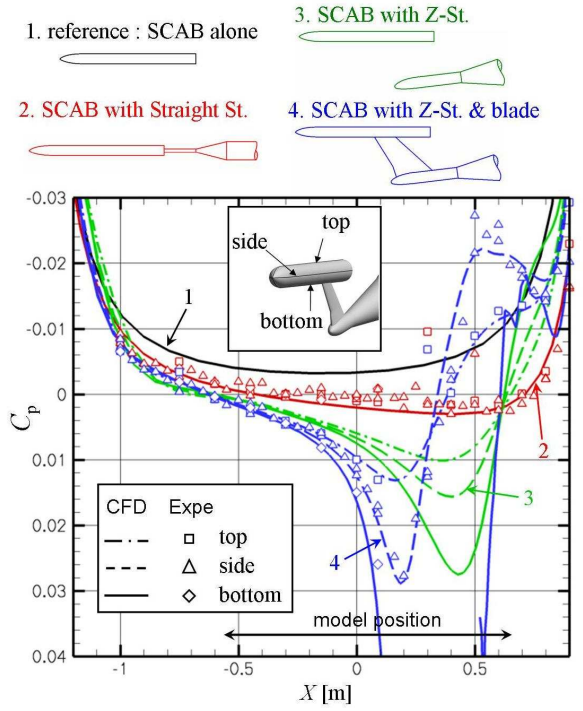

Figure 9: Pressure distribution on the calibration body for various supports (see on top) at M' = 0.85 and α' = 0°, computed by Euler CFD (lines) and measured (symbols)

These computations of the SCAB are repeated for all Mach number, AoA and supports under study to yield a set of ΔM, $\Delta\alpha$ summarised in Figure 10. These corrections are found weakly dependent on the AoA. ΔM increases with Mach number in agreement with usual compressibility rule and $\Delta\alpha$ decreases with Mach number.

c. The choice of a correction method

To conclude with the topic of Mach number and AoA corrections, it is useful to emphasize that the underlying arbitrariness in the choice of ΔM and $\Delta\alpha$ is not critical in theory. Whatever the choice made, the rest of the support correction is just moved into the values of ΔCD, ΔCL and ΔCm. Therefore, two different methods relying on different definitions should yield the same set of final corrected data.

In practice, there are however a couple of conditions to fulfil. Firstly the correction process should indeed be brought to its end, including the accurate determination of force corrections, either by CFD or twin sting tests. Secondly, during this process of deriving force corrections, the Mach number and AoA corrections used should closely represent the wind tunnel's definition of ΔM and $\Delta\alpha$ that was used in the test one aims at correcting. Thirdly, using a definition far from what physical sense suggests (e.g. to the extreme $\Delta M = 0$ and $\Delta\alpha = 0°$) would results in much larger force deviation, which in turn should be determined with higher accuracy. Also, in order to compare other data than forces (such as pressure distribution, which is more difficult to correct), a correction close to the minimum in pressure distortion (*J*-optimal) will be preferred.

The above considerations raise the question of the creation of a common standard in Mach number and AoA corrections. This would ease comparison of data from different wind-tunnels, which would be very useful to the end-users of these facilities. Although this is not the subject of this paper, it is clear that Mach number and AoA corrections due to wall interference raise exactly the same problem.

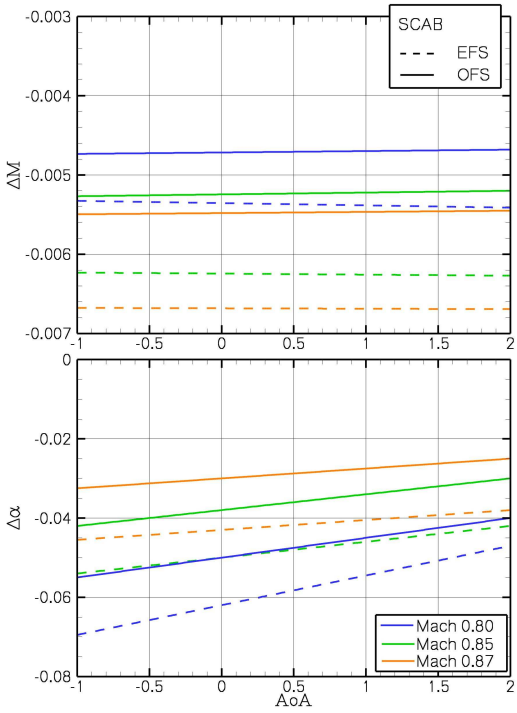

Figure 10: Mach number and AoA corrections determined by calibration method

5. Validation of computed sting effects

Before analyzing predicted sting effects in the next chapter, they are compared with available data from ETW twin sting tests. Comparison is carried out for OFS only, since no experimental data is available for EFS.

a. Assessment and subtraction of VTP forces

It is reminded that the sting interference effect is defined as the difference in wing and fuselage forces between 'sting off' and 'sting on' configurations. Therefore, in order to evaluate this effect, VTP forces should be subtracted from total

model forces in 'sting off' configuration before any comparison with 'sting on' configuration is made.

In CFD results, this is simply achieved by integrating local skin stresses on the fuselage and wing only, therefore explicitly excluding VTP surface.

Concerning wind tunnel test data, forces on the VTP are part of balances measurements. It is therefore required to assess these forces in the conditions of the experiment. These VTP forces are readily available from the results of CFD computations. However, since those computations were performed at a higher Reynolds number than the test, a Reynolds correction on drag is first applied. This correction is evaluated thanks to 2D Euler coupled computations of the flow around the VTP airfoil, and is found to be of about $+1.7\ 10^{-4}$. Finally, the drag coefficient of the VTP in test condition is found to be about $+4\ 10^{-4}$, weakly dependent on Mach number and AoA. VTP lift and pitching moment coefficients are about +0.01 and −0.004 respectively.

b. Sting effect on fuselage pressure

Increments of fuselage pressure due to the OFS are presented in Figure 11. This figure presents pressure data on the top of the fuselage and at 35° from the top, near the sting blade entry. It shows a close agreement between CFD predicted and experimentally measured data on the rear end of the model. It was also the case for other pressure taps all around the rear fuselage. The agreement is less satisfactory close to the middle of the model. This can be explained by the difficulty to properly interpolate experimental pressure data in terms of Mach number and AoA in this region.

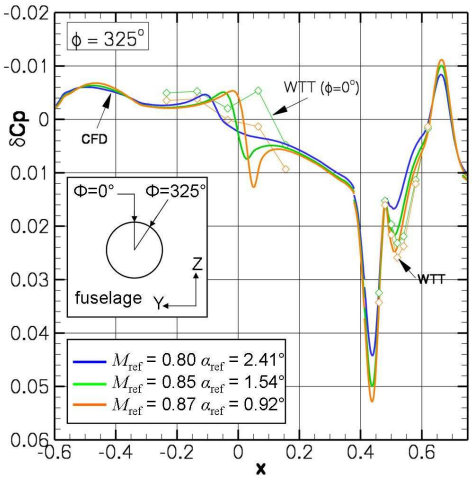

Figure 11: Pressure increment due to OFS on the fuselage as computed (bold lines) and measured (thin lines with symbols) for different flow conditions

c. Sting effect on forces

Experimental data available for the rear body are provided thanks to the balance integrated in the fuselage. The balance reading is corrected (among other phenomena) for split plane pressure. This correction is very large compared to the quantity measured and is the major source of inaccuracy. Indeed, uncertainty associated with the cavity pressure measurement translates into about $\pm 1\ 10^{-4}$ uncertainty for rear body drag.

Forces on the whole model are measured thanks to the two twin-sting boom balances. Because of the large cross-section of the booms, these measurements suffer from the same source of uncertainty as described above, related to the cavity pressure measurements. In addition, because of their size and position, the large twin-sting booms are likely to dramatically change the transonic wing flow field. Strong flow separation and large shock displacement on a significant part of the wing are suspected. Therefore, the effect of the OFS on this distorted flow field may be different from its effect on the free-flight flow-field, especially at flight points where the wing is very sensitive, i.e. at high Mach number at high AoA.

Comparison of sting effect on forces derived by CFD simulations with the experimental sting effect is carried out in Figure 12.

The sting effect on rear fuselage drag is found to be almost independent on AoA, and to increase in Mach number in agreement with usual compressibility rule. This behaviour is well simulated by CFD. The magnitude of the drag effect according to experiment is about $-11\ 10^{-4}$, slightly underestimated by CFD ($-9\ 10^{-4}$).

The drag effect on the complete model is found to be larger and more dependent on AoA and Mach number, both by CFD and experiment. The agreement at Mach 0.85 is still within $2\ 10^{-4}$ up to a lift coefficient of 0.4, then deteriorates to about $5\ 10^{-4}$. At Mach 0.87, the gap between CFD and experiments is constant at about $5\ 10^{-4}$. Considering the above mentioned probable inaccuracy of the experimental sting effect on wing flow, the agreement can be considered as satisfactory.

Plausible explanation for the underestimation of sting effect may be found in the cross-interaction of sting with the wind tunnel walls. Singularity computations [14] of this configuration indeed reveals that the sting effect on the rear fuselage drag is amplified by about 0.4 to $0.6\ 10^{-4}$ (1.6 to $3.5\ 10^{-4}$ for the complete model) depending on the apparent wall porosity.

Concerning the sting effect on lift, it is extremely small on rear fuselage, and also very small on the complete model (less than 0.005). This is well predicted by computations

Finally, the sting effect on pitching moment of the rear fuselage is very small (less than $0.5\ 10^{-3}$) in experiments as in computations. The effect on the complete model evolves between 0 and +0.002 below 0.5 lift coefficient, and is overestimated by 0.001 by simulations.

In general, agreement between experiments and CFD is satisfactory, which validates the simulations carried out.

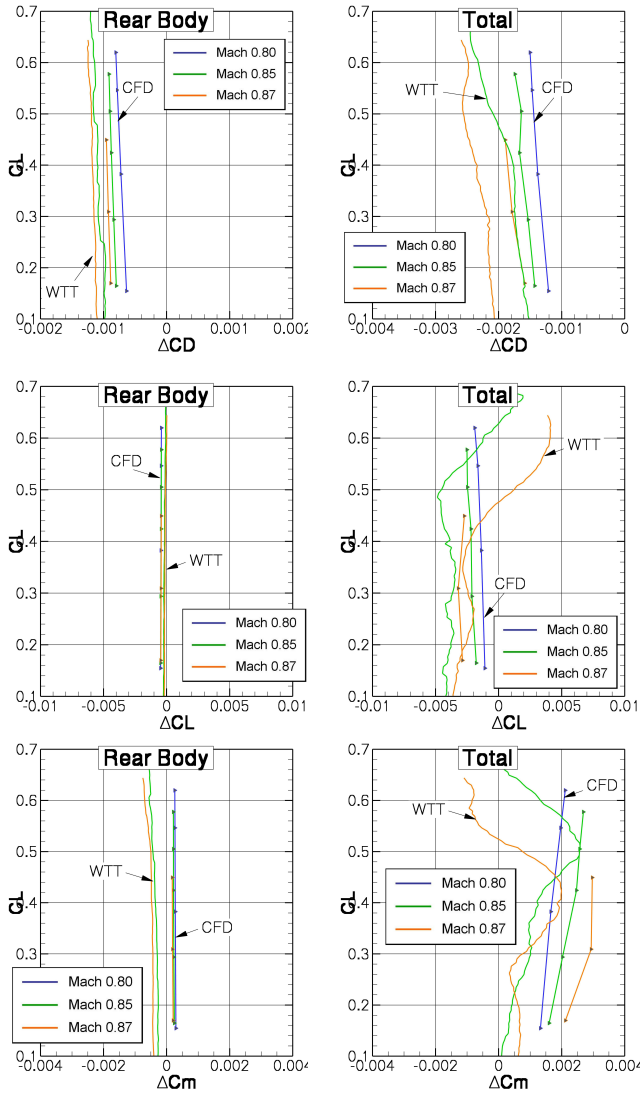

Figure 12: Force increments due to OFS on the rear fuselage (left) and on the complete model (right) as computed by CFD (lines and symbols) and measured (lines). From top to bottom: effect on drag, on lift and on pitching moment

6. Discussion on computed sting effects

This last chapter presents the sting effect Δ*CD*, Δ*CL* and Δ*Cm* derived by CFD for EFS and OFS, in order to discuss this effect and to compare the two different sting designs.

a. Effect on lift and pitching moment

As previously examined, the sting effect on lift coefficient is small for both supports, of the order of −0.005 for EFS and even smaller for OFS. Concerning pitching moment, at Mach 0.85 the effect is also moderate, of about +0.005 for EFS and +0.002 for OFS.

b. Sting effect on drag: buoyancy

In the classical terminology for sting interference, the effect of the sting on drag can be breakdown into on the one side the buoyancy (also called far-field) effect, and on the other side the near-field effect.

The buoyancy is the force generated on a body immerged in a known distribution of one-dimensional pressure field. Generally, a significant part of the support distortion field can be modelled by such a simple pressure distribution $\delta\hat{C}p(x)$ along the fuselage axis. Its effect on the model drag can then be evaluated using the classical Archimedean formula:

$$\Delta CD_{buo} = -\int_{\substack{\text{Model}\\ \text{centreline}}} \frac{d\delta\hat{C}_p}{dx}\frac{S(x)}{S_{ref}}dx.\cos\alpha_{ref},$$

where $S(x)$ is the model cross-section at the x abscissa. At small AoA, $\cos\alpha_{ref} \approx 1$ and in practice the axial force is confused with drag force. Then, the near-field effect is simply what remains from the total effect when buoyancy has been subtracted:

$$\Delta CD_{nf} = \Delta CD - \Delta CD_{buo}.$$

Similarly to what was previously presented for Mach number and AoA corrections, there is a lack of standard in the way to define and to derive the pressure distribution $\delta\hat{C}p(x)$ used to compute buoyancy. This distribution can be measured or computed, it can include the blade or not, etc. Moreover, the buoyancy correction used in wind tunnels may not always draw a distinction between buoyancy generated by the empty tunnel, by the wall and by the support interference. Therefore, the same total sting effect can have several breakdowns, and the buoyancy generated by the support may be confused with other terms. Here again, one understands that care has to be taken when comparing data from different wind tunnels, and also between wind tunnel and CFD.

In this work, the centerline pressure distortion generated by the support $\delta\hat{C}p(x)$ was computed thanks to Euler computations of the flow around isolated stings (without blade). The pressure distribution was then probed along the model centreline.. Also, by integrating separately on the front and the rear fuselage, buoyancy effects can be separated between those two parts.

In Figure 13*a*, the total sting effect is presented, whereas in Figure 13*b* the buoyancy induced by the support has been subtracted from the total support effect to yield the near-field effect. Comparing data from these two figures, one can see that the total sting effect on the front fuselage drag is purely a buoyancy effect, since all ΔCD_{nf} curves are brought to zero (within 10^{-4}), whatever the support, Mach number or AoA. On the other hand, the effect on the rear body drag cannot be fully expressed by a simple buoyancy term, i.e. the rear body is subject to near-field effects (of about $-4\ 10^{-4}$ for OFS and $+7\ 10^{-4}$ for EFS at Mach 0.85).

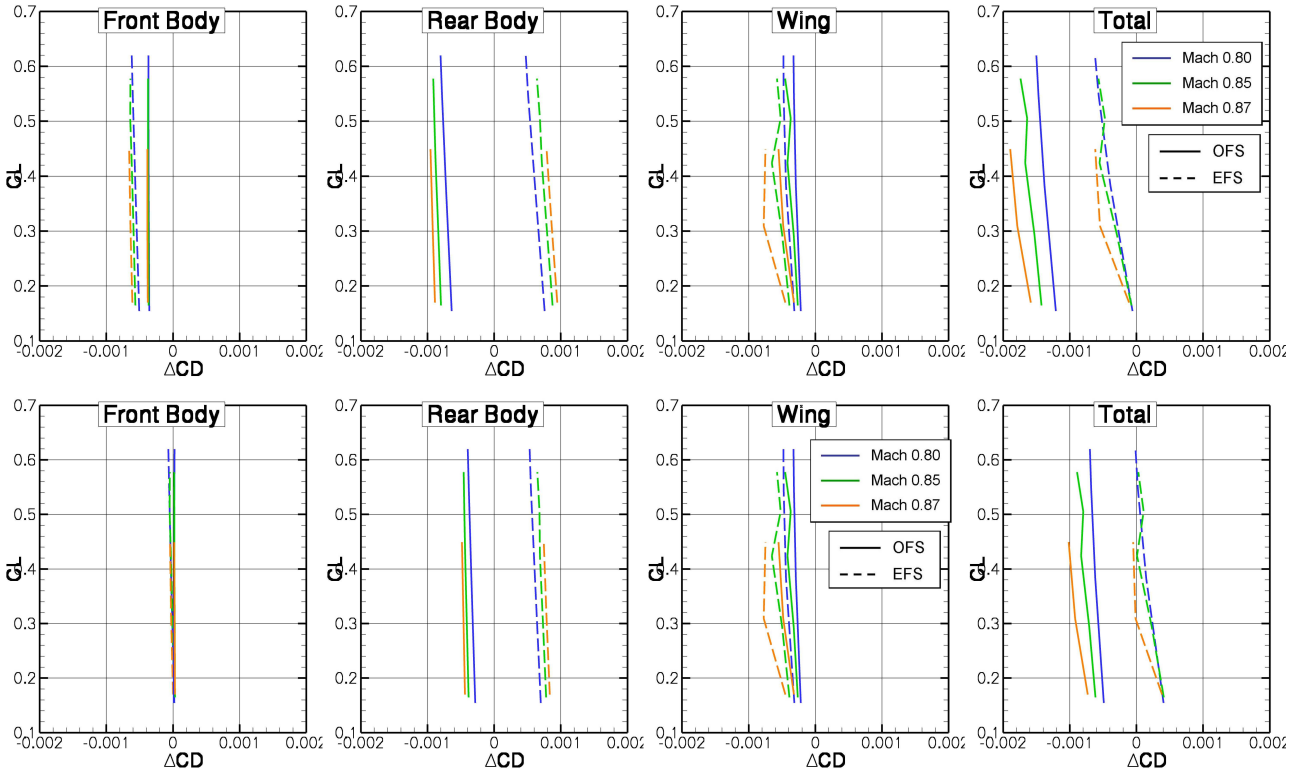

Figure 13: Sting effect on drag
a) total effect
b) near-field effect

c. Sting effect on drag: near-field

Now focusing on buoyancy corrected data of Figure 13*b*, both supports reduce the wing drag by 2 to 8 10^{-4}, the magnitude of this effect being brought down by about 40% thanks to the OFS. Sting effect on the rear body is +6 to +8 10^{-4} for EFS and −3 to −5 10^{-4} for OFS. The flow on the rear body was indeed improved by the OFS as illustrated in Figure 14. However, these results of opposite signs for similar supports show that the near-field drag effect of such blade support is very sensitive to local design and relative position of the blade and fuselage, as was already mentioned in [13].

The total effect of EFS is close to zero as a result of compensation between increased drag of the rear body and lowered drag of wing. On the contrary, for the OFS, the effects on the rear body and the wing are both negative. Although their magnitudes are both lower compared to EFS, they sum up to yield a total effect ranging between −5 and −10 10^{-4}, larger than for EFS. This illustrates the fact that total drag deviation cannot be used as a criterion to assess the quality of a support because of possible compensating contributions.

Results of Figure 13 also show that even well corrected in Mach number and AoA, the sting effect on wing is still of about −3 to −5 10^{-4} at Mach 0.80, and up to −8 10^{-4} at Mach 0.87. Usual twin sting test during which only the rear fuselage is a metric part are unable to detect such an effect on the wing. And even if the wing is a metric part, the transonic flow field might be so much distorted by the twin-sting booms that the support effect on the wing may be different from expected. Therefore, the predicted wing interference could not be properly verified against experimental data.

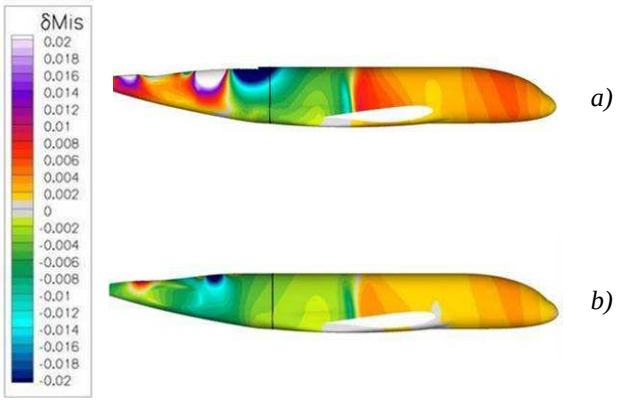

Figure 14: Distortion of isentropic Mach number distribution on the fuselage at M_{ref} = 0.85 and α_{ref} = 1.54°
a) for EFS
b) for ofs

Conclusion

The interference effects of two different fin sting supports for ETW wind tunnel – the existing fin sting (EFS) and the optimised fin sting (OFS) – were assessed by means of CFD computations.

Simulations demonstrated the need to carefully account for Mach number and AoA corrections for each support in order to achieve required accuracy, especially for model with a sensitive design. For

wing-oriented testing, a good Mach number and AoA correction is even more important than the shape of the support itself. For a single flight point, the Mach number and AoA correction minimising wing flow distortion was identified. A method suited for CFD was selected and sting effect was derived for a large range of Mach numbers and AoA.

The sting effects of OFS were validated against twin sting tests carried out at ETW, however at lower Reynolds number. Comparison showed that the drag effect was predicted within about $2\ 10^{-4}$. Remaining discrepancy may partly stem from the cross-interaction effect of the support with the slotted wind tunnel walls, as singularities computations suggest. The small effect of the sting on lift and pitching moment were also correctly predicted (within 0.003 and 0.002 respectively) considering the large contribution of the wing on these terms and the probable experimental inaccuracy of wing flow due to the twin sting booms.

Analysis of CFD results led to the following conclusions. For the front fuselage, the sting effect was shown to be exclusively a buoyancy effect that can be easily corrected whatever the support is. The effect on the rear end of the model is very sensitive to local geometry of the blade and fuselage. The OFS brought significant improvement to this point, although it does not immediately translate in force coefficients. This improvement is however probably insufficient to enable accurate tests of horizontal tail planes using fin sting. Concerning the wing, the more homogeneous flow ensured by the OFS also enables lower interference, although this point has to be confirmed when considering the wind tunnel walls.

A more surprising and problematic finding is that both supports generate significant wing force deviations, up to $-8\ 10^{-4}$ at Mach 0.87, even once well corrected in Mach number and AoA. This support effect on wing is probably difficult to accurately detect by means of twin sting tests, even if the whole model is weighted.

Acknowledgements

The author would like to thank the European Commission for funding this research work within the FLIRET project. The helpful words of advice of J.F. Piat (ONERA), J. Quest, M. Wright and N. Gross (ETW) are gratefully acknowledged.

References

[1] L. Cambier, J.P. Veuillot, "Status of the elsA CFD Software for Flow Simulation and Multidisciplinary Applications", AIAA 2008-664, Reno, January 7-10, 2008.

[2] S. Mouton, "Numerical Investigations of Model Support Interference in Subsonic and Transonic Wind Tunnels", 8th ONERA-DLR Symposium ODAS 2007, Göttingen, October 17-19, 2007

[3] M. Maina, N. Corby, E.L. Crocker, P.J. Hammond, P.W.C. Wong, "A Feasability Study on Designing Model Support Systems for a Blended Wing Body Configuration in a Transonic Wind Tunnel", *The Aeronautical Journal*, January 2006

[4] A. Heidebrecht, "A Numeric Far Field Model for Support Interference Studies in a Slotted Wall Wind Tunnel (ETW)", 2nd International Symposium on Integrating CFD and Experiments in Aerodynamics, RMCS Cranfield University, September 20, 2005

[5] R. Collercandy, B. Marquez, J. Lory, S. Dbjay, L. Espiau, "Application of CFD for Wall and Sting Effects", HiReTT Technical Note HIRETT/TN/AF/RCo/WP2.2/31102003, October 2003

[6] J. Quest, M. Wright, S. Rolston, "Investigation of a Modern Transonic Transport Aircraft Configuration over a Large Range of Reynolds Numbers", AIAA 2002-0422, Reno, January 14-17, 2002

[7] J. Quest, "Tunnel Corrections in ETW", ETW Technical Memorandum ETW/TM/99024, March 1999

[8] J.F. Piat, "Méthodes de correction des effets de parois et de supports utilisées dans les souffleries des GME", ONERA Technical Report RTI 0377/1464 GN, July 1996

[9] R.H. Bush, D.W. Jasper, S.L. Parker, W.W. Romer, P.G. Willhite, "Computational and Experimental Investigation of F/A-18E Sting Support and Afterbody Distorsion Effects", *Journal of Aircraft*, Vol. 33, no. 2, March-April 1996

[10] M. Lyonnet, J.F. Piat, B. Roux, "Model Support Interference Assessment Using a Metric Rear Fuselage and a Twin-Sting at ONERA S2MA Wind Tunnel", International Conference on Experimental Fluid Mechanics, Turin, July 4-8, 1994

[11] P.R. Ashill et al., "Requirements for Experiments for CFD Validation", AGARD AR-303 vol. 1, 1994

[12] F.T. Lynch, R.C.Crites, F.W. Spaid, "The Crucial Role of Wall Interference, Support Interference, and Flow Field Measurements in the Development of Advanced Aircraft Configurations", AGARD CP-535, 1993

[13] A. Elsenaar, S.O.T.H. Han, "A Break-Down of Sting Interference Effects", NLR TP 91220 U, May 1991

[14] X. Vaucheret, "Recent Calculation Progress on Wall Interferences in Industrial Wind Tunnels", *La Recherche Aérospatiale*, no. 3, pp 45-47, 1988

[15] X. Vaucheret, "Effets de parois à S2MA, Influence de dards supports (Essais de maquette F4 de 1980-86-87-88)", ONERA Technical Report RTI 0300/1464 GN, September 1988

[16] D.L. Loving, A.A. Luoma, "Sting-Support Interference on Longitudinal Aerodynamic Characteristics of Cargo-Type Airplane Model at Mach 0.70 to 0.84", NASA Technical Note TN D-4021, July 1967

[17] E.S.Love, "A Summary of Information on Support Interference Assessment at Transonic and Supersonic Speeds", NACA RM L53K12, 1954